Journal of Alloys and Compounds 509 (2011) 7458–7465

Contents lists available at ScienceDirect

Journal of Alloys and Compounds

journal homepage: www.elsevier.com/locate/jallcom

Optical and structural characterisation of pure and Pr^{3+} doped $LaPO_4$ and $CePO_4$ nanocrystals

L. Macalik[a,*], P.E. Tomaszewski[a], A. Matraszek[b], I. Szczygieł[b], P. Solarz[a], P. Godlewska[c], M. Sobczyk[d], J. Hanuza[a,c]

[a] Institute of Low Temperature and Structure Research, Polish Academy of Sciences, ul. Okólna 2, 50-422 Wrocław, Poland
[b] Department of Inorganic Chemistry, Faculty of Engineering and Economics, Wrocław University of Economics, ul. Komandorska 118/120, 53-345 Wrocław, Poland
[c] Department of Bioorganic Chemistry, Faculty of Engineering and Economics, Wrocław University of Economics, ul. Komandorska 118/120, 53-345 Wrocław, Poland
[d] Faculty of Chemistry, University of Wrocław, ul. F. Joliot-Curie 14, 50-383 Wrocław, Poland

ARTICLE INFO

Article history:
Received 27 July 2010
Received in revised form 22 March 2011
Accepted 12 April 2011
Available online 22 April 2011

Keywords:
Rare earth orthophosphates
Nanostructured materials
Hydrothermal synthesis
Optical properties

ABSTRACT

The rod- and stick-shaped nanocrystalline cerium and lanthanum orthophosphates, pure and Pr^{3+} doped, have been synthesised by the hydrothermal method in acidic (pH 1) or alkaline (pH 11) environment. Subsequent calcination of as-obtained powders at different temperatures, 500 and 900 °C, led to the formation of hexagonal and monoclinic phases, respectively. The hexagonal phase at room temperature has been identified as hydrated orthophosphate with zeolite water inside the channels of the structure. The monoclinic phase is free of water.

The average grain size is about 12–30 nm depending on the calcination temperature and preparation conditions. The structural, morphological and optical (vibrational and luminescent) properties have been characterised and their changes due to the temperature and different acidity in the starting materials have been studied.

1. Introduction

Phosphates are known host for the luminescent ions and their optical properties are tunable by rare earth dopants used. Monophosphates doped with rare earth ions have become the centre of great attention due to their favourable optical properties and have been widely studied for application as luminophors, scintillators and laser devices. In a wide class of materials some of them, especially $LaPO_4$ and $CePO_4$ present a broad range of applications in different areas of technological interest. They could be very good hosts for other lanthanide active ions and play role in biological labelling applications. Due to their very high melting point (over 2000 °C), as well as chemical and thermal stability they are considered ceramic matrix for immobilizing high-level radioactive waste.

Monophosphates containing trivalent cerium and terbium ions could be used for lamp phosphor emitting in green [1,2]. The Pr^{3+} ion is a promising optical activator with the possibility of simultaneous blue, green or red emission. Praseodymium concentrated phosphates are characterised by the intense emission with very fast decays due to the allowed electric-dipole 5d–4f transitions which makes them interesting as fast efficient scintillation materials [3–5]. One of the parameters of industrial application of the phosphates is morphology of phosphors what involves studies of improvement of the shape and size of powder particles of the obtained materials [6–8]. The investigations of rare earth-activated lanthanide phosphate-based phosphors pay attention to explore such kind of materials which may improve lifetime and luminescence efficiency for PDP (plasma display panel) applications [9].

The syntheses and thermal stability of various orthophosphates have been reported in numerous papers. Rare earth orthophosphates crystallize in several crystal types: (i) the hexagonal hydrated rhabdophane type ($LnPO_4{\cdot}nH_2O$; $0.5 < n < 1$, the exact water content is not known) for light rare earth elements (La–Gd) and the weinschenkite type ($LnPO_4{\cdot}2H_2O$) for Ln = Dy, Er and Y, (ii) the monoclinic anhydrous monazite type $LnPO_4$ (Ln = La–Gd) and the tetragonal xenotime (zircon) type for heavy rare earth elements (Ln = Tb–Lu, Sc, Y).

A comprehensive review of the monazite- and zircon-type crystals [10] reveals only a few crystal structure solutions, some of them correspond to La or Ce orthophosphates [11–16]. Unfortunately, the exact crystal structure of hydrated phosphate is not known and to our knowledge there is no a similar review concerning rhabdophane-type crystals.

The thermal studies of rhabdophane $LnPO_4{\cdot}nH_2O$ (Ln = La and Ce) [17] showed that two transformations are observed. First one is related to the release of zeolite water at about 220 °C. The second one corresponds to the irreversible structural phase transition at about 620 °C when the anhydrous hexagonal form transforms into

* Corresponding author. Tel.: +48 71 3954184; fax: +48 71 3441029.
E-mail address: L.Macalik@int.pan.wroc.pl (L. Macalik).

0925-8388/$ – see front matter © 2011 Elsevier B.V. All rights reserved.
doi:10.1016/j.jallcom.2011.04.077

the monoclinic monazite phase. The reversibility of the dehydratation was studied by Khorvath et al. [18] up to 250 °C. It should be noted that the temperature reported for these transitions depends on preparing method of hexagonal phases and on its thermal history [19].

In the present paper we focus on the characterisation of $LaPO_4$ and $CePO_4$ nanomaterials undoped and doped with Pr^{3+} ions.

2. Experimental

2.1. Material synthesis

Both hexagonal and monoclinic types of light lanthanide phosphates could be obtained by hydrothermal synthesis [15,20–23]. The conditions of synthesis, i.e. temperature and the pH value of solution influenced the type of obtained product. Nanoparticles of cerium and lanthanum orthophosphates, pure and slightly doped −1 at.% – with Pr^{3+} ions, were prepared by the long- and short-lasting low-temperature hydrothermal methods.

In the former method, high purity $LnCl_3{\cdot}7H_2O$, where Ln = La, Ce and Pr, were dissolved in 0.1 M HCl and the appropriate volume of crystalline H_3PO_4 was added. The mixture with pH 1 was transferred into a Teflon-lined stainless steel vessel and the hydrothermal reaction lasted at 100 °C for 24 h. The autoclave was naturally cooled to room temperature. The obtained powders were separated by centrifugation and washed several times with double distilled water and methanol. Similar method was used by Ferhi et al. [20] to obtain lanthanum phosphate microcrystalline powder doped with Eu^{3+}. For samples obtained in the alkaline environment the stoichiometric amounts of lanthanide chlorides and crystalline H_3PO_4 were dissolved in distilled water and the pH value of the solution was kept about three by adding 1 M HCl. After half an hour, the clear solution was heated to 70 °C and the pH value was adjusted dropwise to 11 with 1 M NaOH. The opalescent colloid was subsequently transferred into a Teflon-lined stainless steel vessel and the hydrothermal reaction was run in the same manner as for acidic condition of reaction.

The powders of $LaPO_4$ and $CePO_4$ were also obtained under short-lasting hydrothermal conditions. The chemical reagents, La(III) or Ce(III) nitrate hexahydrate and diammonium hydrogen phosphate, were used in stoichiometric molar ratios with the concentration of lanthanides of 0.04 mol/dm^3. The lanthanum/cerium nitrate and the phosphate precursors were diluted with water to obtain 50 ml of milky solution. As obtained sols were products of acidic reaction (pH 1). The alkaline solutions were derived in a similar way, except for addition of ammonia to achieve pH 11. The sols were aged for 24 h before the hydrothermal treatment. Unfortunately, the doping with Pr^{3+} was unsuccessful using this method. The hydrothermal reactions were performed in a Magnum II autoclave (Ertec, Poland) with heating of the samples by microwaves of the maximal power of 600 W. The syntheses were controlled by measuring of total pressure in the Teflon reactor. The hexagonal type phosphates were obtained by heating of the sols under p_{max} = 20 bar for 15 min. As obtained fine precipitates were filtered and washed several times with distilled water.

The final product, powders in the nanocrystalline form with hexagonal symmetry, was obtained by drying the as-synthesized powders at 100 °C for 2 h and by subsequent calcination at 500 °C for 24 h in an electric furnace in a nitrogen atmosphere (N_2). The monoclinic samples were obtained by calcination of the as-synthesized powders at 900 °C for 24 h in a N_2 atmosphere. The obtained samples were used for further investigation.

2.2. X-ray powder diffraction

X-ray powder diffraction patterns (XRD) were recorded at room temperature by using STADI-P powder diffractometer (STOE, Germany) working in the transmission geometry and equipped with a linear 140°-PSD detector. CuKα_1 radiation (λ = 1.54056 Å) in the 2Θ range from 10° to 65° with a step of 0.03° a flat rotating sample holder was used. DICVOL04 [24] was used for indexing the X-ray powder diffraction patterns. The structure solution was carried out using FullProf package [25].

The average size of nanocrystallites was estimated from the broadening of the X-ray diffraction lines using the Scherrer equation $D = K\lambda/(\beta \cos \Theta)$, where D is the diameter of the crystallite (in the approximation of a spherical shape), λ is the X-ray wavelength, β is the full width at half maximum (FWHM) of the diffraction line (in radians) and Θ is the Bragg angle of diffraction peak [26,27]. The Scherrer constant K is conventionally set to 1.0 [28]. The contribution of the instrumental broadening was removed by subtracting the FWHM of the respective line observed for well-annealed bulk crystals. The Halder–Wagner parabolic approximate relation, $\beta = B - b^2/B$, was used β is the FWHM of the true diffraction profile, B and b are the measured FWHM of the equivalent diffraction lines in the specimen and the reference sample, respectively [27,28].

2.3. Electron microscopy studies

The morphology and particle size of the phosphates were determined using a transmission electron microscopy (TEM) technique. The TEM specimens were prepared by dispersing a small amount of the nanocrystalline powder in pure ethyl alcohol with ultrasonic agitation. A droplet of the suspension was deposited on a copper microscope grid covered with carbon thin film. The grains on the supported films were then examined using conventional TEM (Tesla BS 500, operated at 90 kV). The microstructure was studied by high-resolution TEM (HRTEM, Philips CM20 SuperTwin operating at 200 kV).

2.4. Spectroscopic measurements

The infrared absorption spectra were measured at room temperature using a Biorad 575C FT-IR spectrometer in the spectral range of 50–4000 cm^{-1}. KBr pellet and the Nujol mull suspension technique were applied to measurements for the mid (MIR) and far (FIR) infrared range, respectively. Room temperature Raman spectra were recorded in the spectral range of 80–4000 cm^{-1} with a Bruker RFS 100 FT-Raman Spectrometer using the back scattering arrangement. The 1064 nm line of Nd:YAG laser as an excitation source and a liquid nitrogen-cooled Ge detector were used. Both IR and Raman spectra were recorded with a spectral resolution of 2 cm^{-1}.

The luminescence and excitation spectra were gathered with a Hamamatsu R-955 PMT using one channel 750 focal length a Dongwoo Optron spectrophotometer (model DM711). To excite the sample a 180 W ozone-free lamp (Dongwoo Optron) was used. All measurements were performed at room temperature.

In luminescence decay time measurements, short pulses (4 ns) produced by an optical parametric oscillator OPO (Continuum, Surelite I) pumped by the third harmonic of Nd:YAG laser were used to excite directly luminescence levels. The decay signal was detected, averaged and stored with a Tektronix TDS 3052 digital oscilloscope; the all decay data consisted of ten thousand points. The fits of experimental decay curves were done using the Microcal Origin v5.0 software; the amplitude of the curves was calibrated to thousand. The analysed multiplets ($^3P_0$ and $^1D_2$) were excited directly to avoid the influence of over-lying multiplets onto decay curves profiles of measured levels. Due to non-exponential character of decay curve of the $^1D_2$ curves the mean lifetime (τ_m) of this multiplet can be evaluated following the Inokuti–Hirayama formula [29]:

$$\tau_m = \frac{\int_{t=0}^{\infty} tI(t)dt}{\int_{t=0}^{\infty} I(t)dt} \quad (1)$$

where I is the intensity of luminescence and t represents time.

3. Results and discussion

3.1. Structural considerations

Analysis of the X-ray powder diffraction patterns of the orthophosphate nanopowders shows that the investigated samples are free of impurity phases and they are independent of the crystallisation method used. The as-synthesized phosphates have hexagonal symmetry both for pH 11 and pH 1 for the starting solution. All diffraction peaks for the samples calcined at 500 °C and 900 °C could be indexed in the hexagonal and monoclinic unit cells, respectively. Fig. 1 shows the X-ray powder diffraction patterns of as-synthesized $CePO_4$ and hexagonal $CePO_4$ synthesized under the acidic or alkaline conditions and subsequently calcined at 500 °C. The monoclinic $CePO_4$ synthesized under the acidic or alkaline conditions and subsequently calcined at 900 °C are also presented. For comparison, the diffraction patterns of corresponding crystals are added. The praseodymium dopant is not the reason for the shift of the diffraction peaks. XRD patterns for $LaPO_4$ are shifted towards the lower degrees in comparison to the $CePO_4$ apart from the type of phosphate. In Figure 1 the $LaPO_4$:Pr^{3+} obtained under pH 1 and pH 11 is shown as an example.

Due to the rather poor quality of the X-ray powder diffraction patterns (*n.b.* obvious for nanocrystalline species), solution of the structures is difficult when using a routine procedure. Fortunately, the structures of our samples similar to those known from literature: hexagonal [11] and monoclinic [14]. However, the exact crystal structure of hydrated orthophosphate is not known. The key paper by Mooney [11] gives the positions of atoms except those of zeolite water. The same rigid framework as for our hexagonal ortophosphates was found in the structure of $KCaNd(PO_4)_2$ [30] where K^+ ions are in the channels instead of water molecules. Unfortunately, the use of such model for the samples calcined

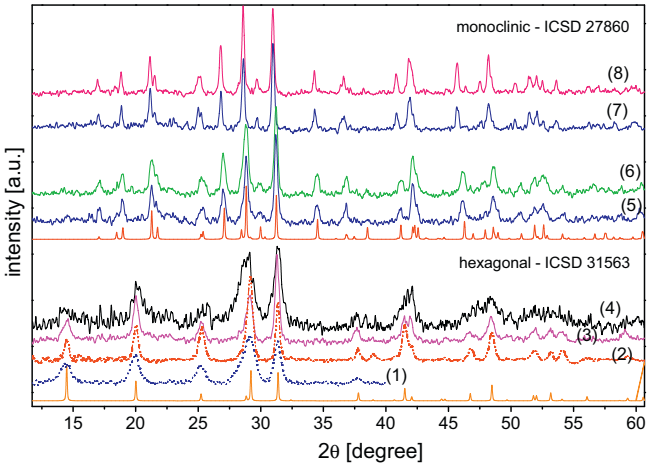

Fig. 1. X-ray powder diffraction patterns of the orthophosphate nanopowders with the patterns of corresponding crystals [11,14] for comparison: as-synthesized $CePO_4$ (pH 11) – (1), as-synthesized $CePO_4$ (pH 1) – (2), $CePO_4{\cdot}nH_2O$ (pH 1, 500 °C) – (3), $CePO_4{\cdot}nH_2O$ (pH 11, 500 °C) – (4), $CePO_4$ (pH 1, 900 °C) – (5), $CePO_4$ (pH 11, 900 °C) – (6), $LaPO_4{:}Pr^{3+}$ (pH 1, 900 °C) – (7) and $LaPO_4{:}Pr^{3+}$ (pH 11, 900 °C) – (8).

at 500 °C, does not give satisfactory agreement between calculated and observed diffraction patterns. A slight improvement in structure solution was noted only. Thus, the problem of the exact position of water molecules in our nanocrystals is still open.

The presence of water in the structure indicates a very unstable form. The hexagonal type orthophosphates are assumed to be metastable compounds whose structure is stabilised by water molecules of zeolitic nature. In such a case, the release of water under heating at temperatures higher than 250 °C should result in polymorphic transformation with subsequent monazite formation. Under our study phosphates of rhabdophane-type were hydrated (see also for the FTIR analysis results) in spite of the samples calcination at 500 °C. Thus, the reversibility of dehydration is possible even up to 500 °C which exceeds the temperature regime of the rhabdophane existence range [18].

In the case of samples affected by the thermal treatment at 900 °C, the structure is similar to that well known from literature [13,14]. It is monoclinic $P2_1/n$ structure with the lattice parameters of about $a = 6.8$ Å, $b = 7.0$ Å, $c = 6.46$ Å and $\beta = 103.5°$. It should be noted that the monoclinic structure has a more compact atom arrangement than the hexagonal one justifying the irreversibility of transition at about 620 °C. Detailed considerations will be published elsewhere. However, the monoclinic phase could be obtained by the hydrothermal synthesis at temperature about 200 °C [20].

The grain sizes of the obtained samples and the morphology of crystallites depend on the growth conditions (pH value, temperature of hydrothermal treatment and calcination) as well as on the dopants used. Upon analysis of the X-ray diffraction lines using the Scherrer equation the average size of nanocrystallites was estimated. The samples received from acidic solution (pH 1) and calcined at 500 °C consist mainly of rod-like shape nanometric

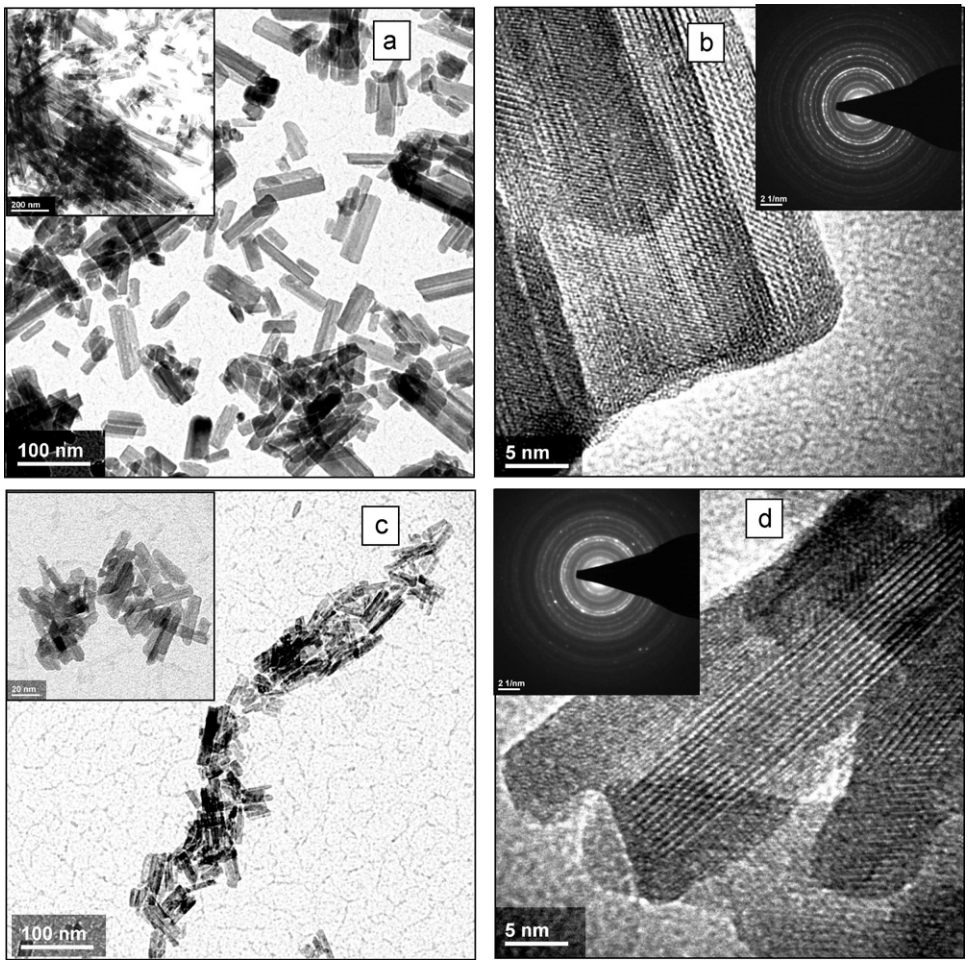

Fig. 2. TEM images of the as-synthesized phosphates by hydrothermal treatment: (a) $CePO_4$ obtained under pH 1 (inset: a fragment with nanowires, scale of 200 nm), (c) $CePO_4$ obtained under pH 11 (inset: a fragment with scale of 20 nm) and HRTEM images of single nanorods with the corresponding selected area electron diffraction (SAED) patterns in insets: (b) $CePO_4$ obtained under pH 1, (d) $CePO_4$ obtained under pH 11.

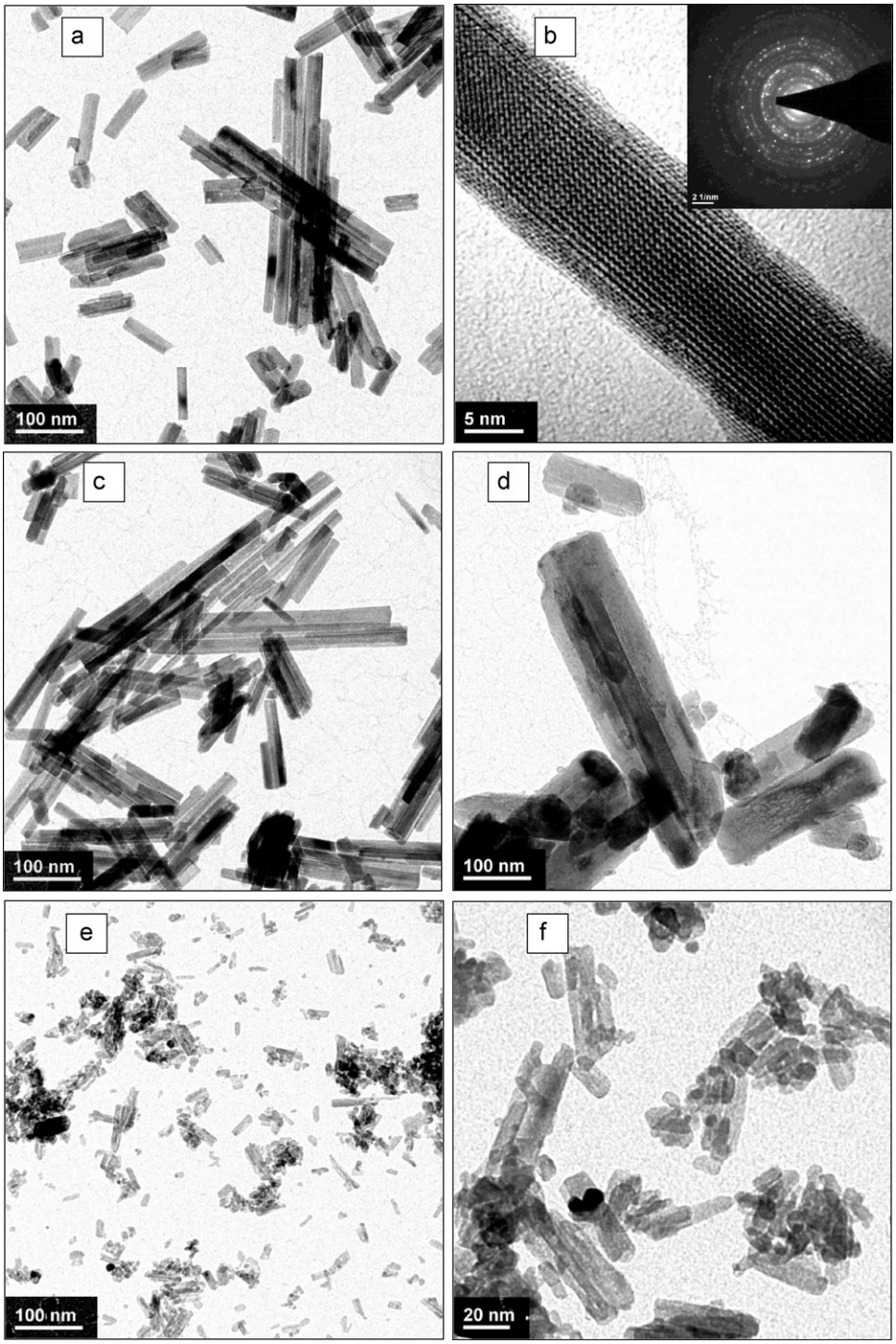

Fig. 3. TEM images of the hexagonal phosphates: (a) $CePO_4$:Pr obtained under pH 1, (c) $CePO_4$ obtained under pH 1, (d) $CePO_4$:Pr obtained under pH 1 and long-lasting hydrothermal method, (e) and (f) $CePO_4$ obtained under pH 11 and (b) HRTEM image of single nanorod with the corresponding SAED pattern in insets for $CePO_4$ obtained under pH 1.

particles with linear dimensions of about 20 nm × 20 nm × 40 nm for pure samples, and 20 nm × 20 nm × 100 nm for the samples doped with praseodymium. On the other side, the samples crystallised at pH 11 contain spherical grains with a mean diameter of about 12 nm. The grains of the samples treated at 900 °C have nearly spherical shape with the diameter of about 30 nm for all samples independently of pH and the dopant presence. The change of morphology from rod-like to round-shaped grains in the samples received at pH 1 was also observed in micropowders obtained by ball milling. Corresponding change in morphology was not observed for the samples obtained at pH 11 [19].

The results obtained from the Scherrer equation were verified by microscopy studies. It appeared that the commonly used Sherrer method was very approximate and it could not be applied to the particles with the lengthened shape. It seems that all types of the obtained phosphates in this investigation crystallize in rod-like shape nanometric particles. TEM images of the as-synthesized phosphates are presented in Fig. 2. The as-synthesized $CePO_4$ phos-

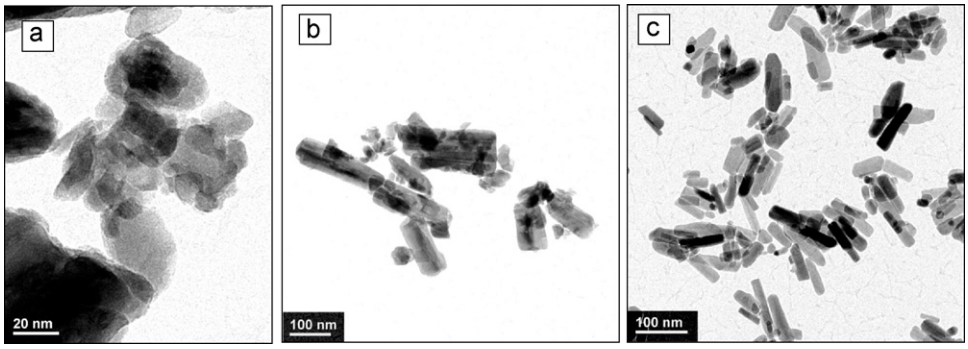

Fig. 4. TEM images of the monoclinic phosphates: (a) and (b) $CePO_4$ obtained under pH 1 and (c) $CePO_4$ obtained under pH 11.

phate obtained under pH 1 consists almost entirely of nanorods with diameters close to 20 nm. However, separate agglomerates of very long nanowires with lengths up to a micrometer appeared in places as it is seen in the inset of Fig. 2a. Particles obtained under pH 11 are considerably smaller with diameters less than 10 nm. Their distribution is rather uniform (Fig. 2c).

HRTEM images and the selected area electron diffraction (SAED) patterns (Fig. 2b and d with insets) taken from a single rod show clearly resolved planes indicating the single crystallisation and that the direction of the rod growth is along the *c*-axis. The same results are observed for the other phosphates calcined both at 500 and 900 °C.

Fig. 3 presents TEM images of the hexagonal phosphates. It is seen that Pr^{3+} ions dopant does not change the morphology of nanoparticles (Fig. 3a and c). Mainly the rod-like shape particles obtained at pH 1 have about 20 nm of diameter and tens nm of length although, the longer rods with several hundred nm of length also appeared. Nanorods obtained by the long-lasting hydrothermal method have slightly bigger diameters and there are more very short rods (Fig. 3d). Hexagonal phosphates obtained at pH 11 have still the same morphology but their diameters are considerably smaller (Fig. 3e and f). HRTEM and SAED results confirm the observations for the as-synthesized phosphates (Fig. 3b).

TEM images for the monoclinic phosphates presented in Fig. 4 show that particles morphology remained intact after calcination at 900 °C. Nanorods of samples obtained at pH 1 have a little bigger diameters in comparison with the samples obtained at pH 11.

3.2. Vibrational studies

Infrared spectra of nanocrystalline orthophosphates are shown in Figs. 5 and 6 for hexagonal and monoclinic crystals, respectively. The bands are characteristic for phosphates with the PO_4 tetrahedra. The space group $P6_222$ for hexagonal and $P2_1/n$ for monoclinic phosphates was postulated by Mooney [11,31]. The spectra were discussed with reference to tetrahedral molecular symmetry and site symmetry occupied by phosphor [19]. Table 1 presents the correlation diagram for the PO_4 tetrahedra [32]. The normal vibrations of the PO_4 species for phosphates calcined at 900 °C appear in the following regions: ν_1 mode (P–O symmetric stretching) at about 956 cm^{-1}, ν_3 mode (P–O asymmetric stretching) at about 994, 1025, 1062 and 1094 cm^{-1} and ν_4 mode (O–P–O asymmetric bending) at about 541, 565, 580 and 613 cm^{-1}. For phosphates calcined at 500 °C only three bands are observed in the range of ν_4 vibration modes. Moreover, for the monoclinic orthophosphate the ν_2 modes (O–P–O symmetric bending) at about 491 cm^{-1} can be observed in some extent, while for the hexagonal phosphate ν_2 vibration modes are not observed in the studied wavenumber range. Further, the band of ν_1 mode is very weak and the range of ν_3 mode is broad and not fully resolved. It seems to confirm that the site symmetry for the PO_4 polyhedron could be D_2 in the case of hexagonal phosphates and C_2 for monoclinic ones [19,30].

The Raman spectra shown in Fig. 7 exhibit strong modes between 390 and 1100 cm^{-1} related to vibrations of the PO_4 tetrahedral. For the monoclinic phosphates the spectra are rich especially in the ν_2 and ν_4 mode range situated at 390–490 and 520–630 cm^{-1}, respectively. The ν_1 mode situated at 967 cm^{-1} for lanthanum and 971 cm^{-1} for cerium is very strong and ν_3 mode is composed with five bands situated at 991, 1024, 1055, 1065 and 1073 cm^{-1}. For the hexagonal phosphate the bands in the Raman spectra are very weak and hardly detected. Only two peaks are strong enough to be well detected: 468 cm^{-1} for ν_2 and 979 cm^{-1} for ν_1 modes.

The hexagonal structure of $LnPO_4 \cdot nH_2O$ (Ln = La – Nd) is built of PO_4 tetrahedra and LaO_8 polyhedra connected together and form chains which are linked by the P–O–Ln bonds leaving an open

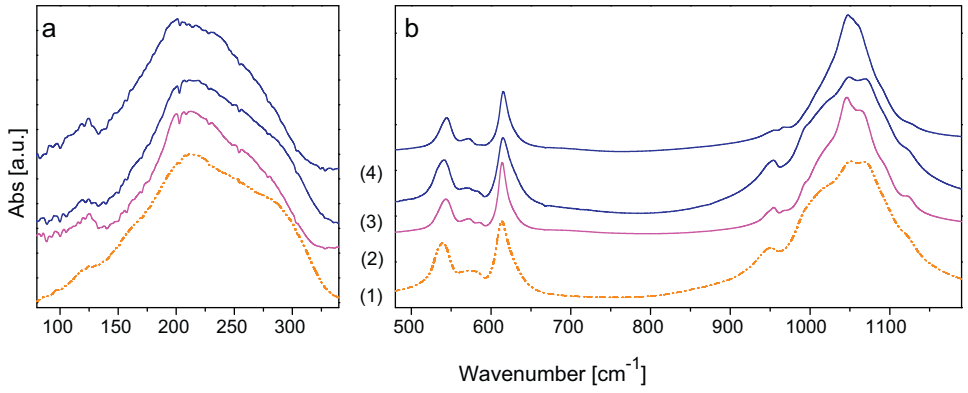

Fig. 5. FIR (a) and MIR (b) spectra of the hexagonal nanopowders: $LaPO_4 \cdot nH_2O:Pr^{3+}$ (pH 11) – (1), $CePO_4 \cdot nH_2O$ (pH 1) – (2), $CePO_4 \cdot nH_2O$ (pH 11) – (3) and $CePO_4 \cdot nH_2O:Pr^{3+}$ (pH 1) – (4).

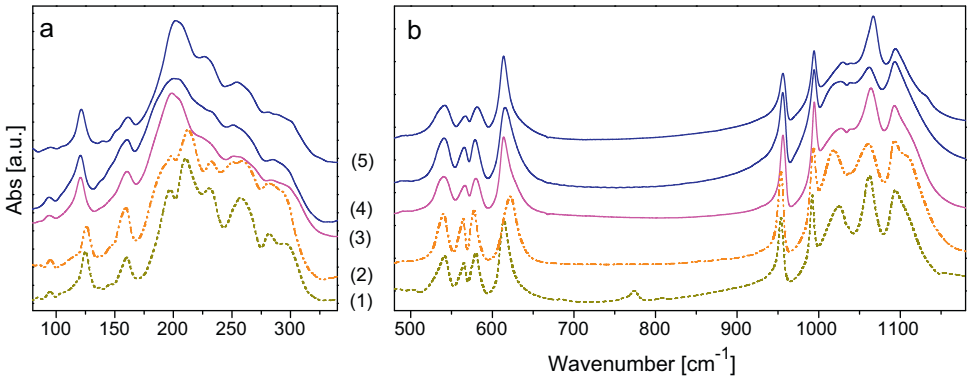

Fig. 6. FIR (a) and MIR (b) spectra of the monoclinic nanopowders: $LaPO_4$:Pr^{3+} (pH 1) – (1), $LaPO_4$:Pr^{3+} (pH 11) – (2), $CePO_4$ (pH 1) – (3), $CePO_4$ (pH 11) – (4) and $CePO_4$:Pr^{3+} (pH 1) – (5).

Table 1
Correlation between the tetrahedral PO_4 molecular symmetry and possible site symmetries occupied by the phosphor in orthophosphate.

T_d		D_2		C_2	
A_1(RS)		A(RS)		A(IR, RS)	ν_1
E(RS)		A(RS) A(RS)		A(IR, RS) A(IR, RS)	ν_2
F_2(IR, RS)		B_1(IR, RS) B_2(IR, RS) B_3(IR, RS)		A(IR, RS) B(IR, RS) B(IR, RS)	ν_3
F_2(IR, RS)		B_1(IR, RS) B_2(IR, RS) B_3(IR, RS)		A(IR, RS) B(IR, RS) B(IR, RS)	ν_4

channels along the hexagonal *c* axis. These channels could be occupied by the water molecules which would stabilise the structure [11]. Hexagonal phosphates are hydrated what is confirmed by the appearance of strong absorption bands in IR spectra (this range is not presented in Fig. 5). The O–H stretching modes are located at 3471 and 3514 cm^{-1}, while the bending modes are at 1630 cm^{-1}. These bands are not observed for monoclinic orthophosphates indicating loss of zeolite water during heating the sample above 600 °C. The absence of band of water vibration in the 700–800 cm^{-1} range indicates the zeolitic nature of water [20].

3.3. Luminescence studies

The luminescence measurements results for nanocrystalline orthophosphates doped with 1 at.% Pr^{3+} are shown in Figs. 8 and 9, respectively. Fig. 8 presents the excitation spectra of Pr^{3+} luminescence in $LaPO_4$ monitored at 607 nm. The shape of the bands of the monoclinic compounds (*i.e.* the samples calcined at 900 °C) is very similar independently of the crystal growth conditions what confirms that these nanocrystals have the same structure. The spectra are composed of the well-separated bands reflecting transitions:

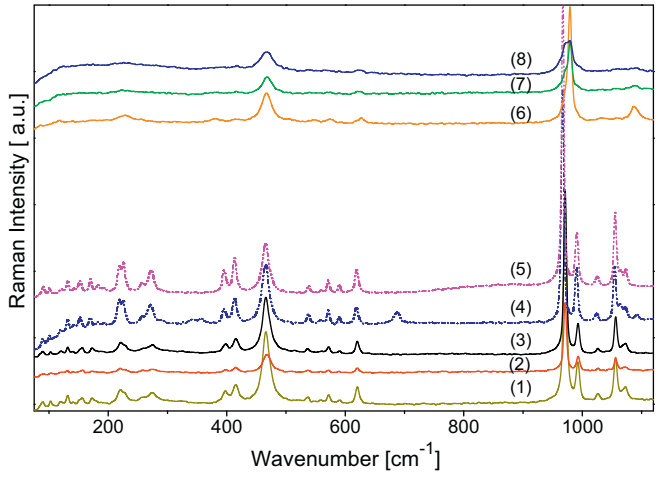

Fig. 7. Raman spectra of the hexagonal and monoclinic nanopowders: $CePO_4$:Pr^{3+} (pH 1, 900 °C) – (1), $CePO_4$ (pH 1, 900 °C) – (2), $CePO_4$ (pH 11, 900 °C) – (3), $LaPO_4$:Pr^{3+} (pH 1, 900 °C) – (4), $LaPO_4$:Pr^{3+} (pH 11, 900 °C) – (5), $CePO_4{\cdot}nH_2O$:Pr^{3+} (pH 1, 500 °C) – (6), $CePO_4{\cdot}nH_2O$ (pH 1, 500 °C) – (7) and $CePO_4{\cdot}nH_2O$ (pH 11, 500 °C) – (8).

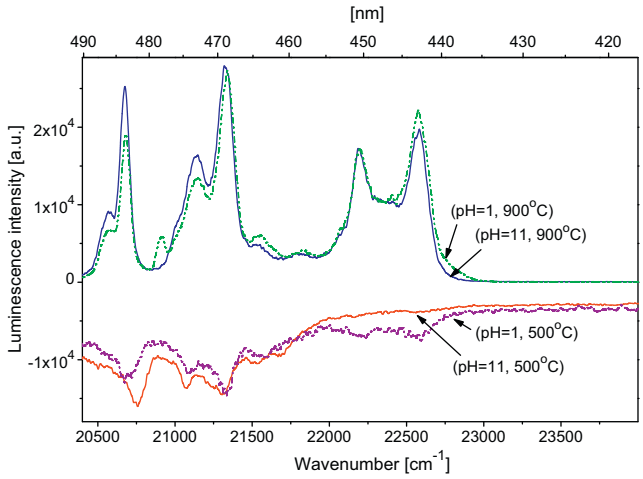

Fig. 8. The excitation spectra of $LaPO_4$:Pr^{3+} obtained at pH 1 and 11 and calcined subsequently at 500 and 900 °C, respectively; λ_{lum} = 607 nm. The spectra of the samples calcined at 500 °C are shown as inverted (upside down) for better clarity of the figure.

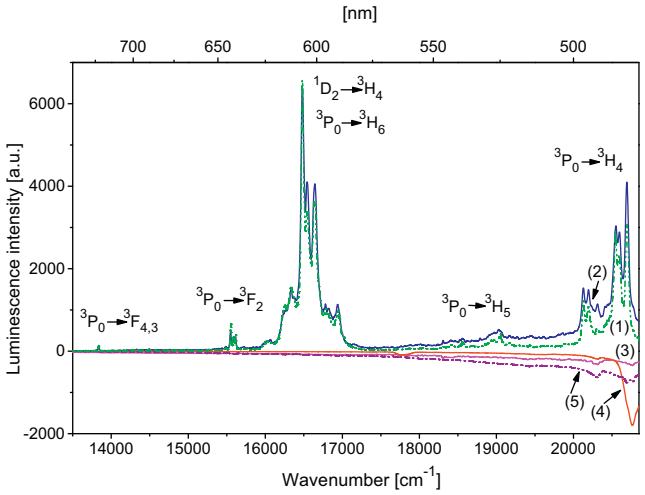

Fig. 9. The emission spectra of $LaPO_4:Pr^{3+}$ for the samples obtained at: (pH 1, 900 °C) – (1), (pH 11, 900 °C) – (2), (pH 11, 500 °C) – (4), (pH 1, 500 °C) – (5) and of $CePO_4:Pr^{3+}$ for samples obtained at (pH 1, 900 °C) – (3); λ_{exc} = 455 nm. Some spectra of the samples are shown as inverted (upside down) for better clarity of the figure.

$^3H_4 \rightarrow {}^3P_0$ with maxima located at 20 570 and 20 675 cm^{-1} (486 and 484 nm), $^3H_4 \rightarrow {}^3P_1, {}^1I_6$ with maxima at 21 145 and 21 340 cm^{-1} (473 and 469 nm) and $^3H_4 \rightarrow {}^3P_2$ with maxima at 22 190 and 22 580 cm^{-1} (451 and 443 nm). However, a supplementary weak band situated at 20 905 cm^{-1} (478 nm) is observed in the spectrum of the sample obtained at pH 1. It could be of vibronic nature and its appearance may suggest that conditions of the crystallisation affect phonon properties. The excitation spectra of praseodymium doped samples calcined at 500 °C are composed of rather weak broad bands. The significantly lower intensity of the lines may indicate that the water molecules present in the hexagonal samples play a meaningful role in the luminescence quenching. In addition, nearly not visible bands in the range of 440–450 nm for the samples obtained at pH 11 testify that the environmental conditions of crystal growth have also an influence on optical properties of the obtained material.

Any attempt of recording of the excitation spectra of $CePO_4$ doped with 1 at.% of Pr^{3+} was unsuccessful for the both samples calcined at 500 °C and 900 °C, apart from the pH value of the reagent solution. Even the experiment under nitrogen atmosphere could not lead to any result because the samples became yellow-brown.

The emission spectra of $LnPO_4$ doped with Pr^{3+} ions are presented in Fig. 9. Two bands dominate for lanthanum samples calcined at 900 °C. The first one is related to the emission originated at the $^3P_0$ level to the ground level $^3H_4$ and it is composed of several narrow lines situated at 20 675, 20 575, 20 535, 20 295, 20 175 and 20 115 cm^{-1} (484, 486, 487, 493, 496 and 497 nm, respectively). The second main band may be assigned to the $^1D_2 \rightarrow {}^3H_4$ transition and is composed of lines situated at 16 920, 16 795, 16 760, 16 625, 16 525 and 16 460 cm^{-1} (591, 595, 597, 602, 605 and 607 nm, respectively). Weaker bands are related to the transitions from $^3P_0$ to $^3H_5$ (19 000 cm^{-1}/526 nm), $^3F_2$ (15 500 cm^{-1}/645 nm), and $^3F_{3,4}$ (13 700 cm^{-1}/730 nm). All mentioned transitions were hardly visible in cerium orthophosphate calcined at 900 °C and analogous lanthanum orthophosphates calcined at 500 °C. On the other hand, for the hexagonal $LaPO_4 \cdot nH_2O$ obtained at pH 11, a broad band with maximum situated at 20 730 cm^{-1}/482 nm can be observed. The nature of this band is unclear now, it may be due to scattering of excitation light. In the excitation spectrum no transfer from cerium d-levels to Pr^{3+} multiplets is observed.

Table 2
The lifetimes of the $^1D_2$ and $^3P_0$ multiplets of Pr^{3+} (1 at.%) recorded for samples of cerium and lanthanum orthophosphates.

Sample	Temperature of calcination (°C)	pH	$^1D_2$ (μs)	$^3P_0$ (μs)
$CePO_4 \cdot nH_2O:Pr^{3+}$	500	1	0.99[a]	0.97[a]
$CePO_4:Pr^{3+}$	900	1	31.95	0.94[a]
$LaPO_4 \cdot nH_2O:Pr^{3+}$	500	1	29.20	0.94[a]
$LaPO_4:Pr^{3+}$	900	1	62.92	2.49
$LaPO_4 \cdot nH_2O:Pr^{3+}$	500	11	26.35	0.94[a]
$LaPO_4:Pr^{3+}$	900	11	74.81	2.34

[a] Time constant of the measurement setup of lifetime is ~0.9 μs.

3.4. Dynamics of excited states

The lifetimes of the $^1D_2$ strongly depend on the calcination temperature and matrix composition. The detailed data were gathered and presented in Table 2 and Fig. 10. The lifetime of the $^1D_2$ multiplet in the case of cerium compound calcined at 500 °C is short, not longer than 1 μs. With increase of the calcination temperature to 900 °C it becomes longer by about 30 times. Unfortunately, we were not able to record the lifetime of this multiplet for cerium phosphate sample synthesised at pH 11. That may lead to suggestion that at low calcined temperature small amount of water oxidize Ce^{3+} to Ce^{4+} which manifest in the $^1D_2$ luminescence quenching that might be removed with calcination at 900 °C (sample synthesized at pH 1). In the case of high concentration of OH^- ions the number of oxidized Ce^{4+} ions is too big and such samples do not show luminescence even after calcination at 900 °C [33,34].

The influence of calcination temperature and pH on the lifetimes of the $^1D_2$ multiplet of Pr^{3+} in lanthanum orthophosphate compounds is much weaker. They are found to be about 27 μs for the samples calcined at 500 °C, whereas they become about twice as long for the samples calcined at 900 °C. All recorded decay profiles of the $^1D_2$ multiplet were non-exponential, this may suggest that the $^1D_2$ multiplet in studied phosphates is concentration dependent.

The lifetimes of the $^3P_0$ multiplet are rather short. For the all analysed samples calcined at 500 °C they are not longer than 1 μs but for the samples calcined at 900 °C the lifetimes are twice as long except for the cerium orthophosphate, where value of the lifetime is still about 1 μs (Table 2 and Fig. 11.).

Similar behavior has been observed by Łempicki and McCollum in $K_5CeLi_2F_{10}$, $K_5LaLi_2F_{10}$ and $K_5GdLi_2F_{10}$ hosts doped with Pr^{3+} [35]. It was shown that Ce^{3+} matrix reduces efficiently the $^3P_0$ emission by about a factor of 100 compared to either Gd^{3+} or La^{3+}. The

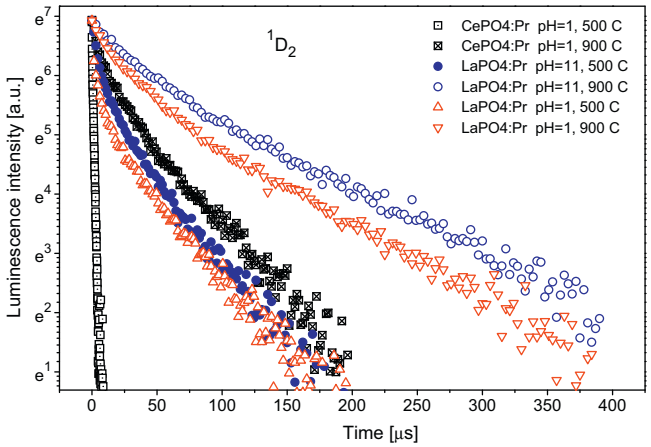

Fig. 10. Lifetimes of the $^1D_2$ multiplet of Pr^{3+} in lanthanum and cerium orthophosphates.

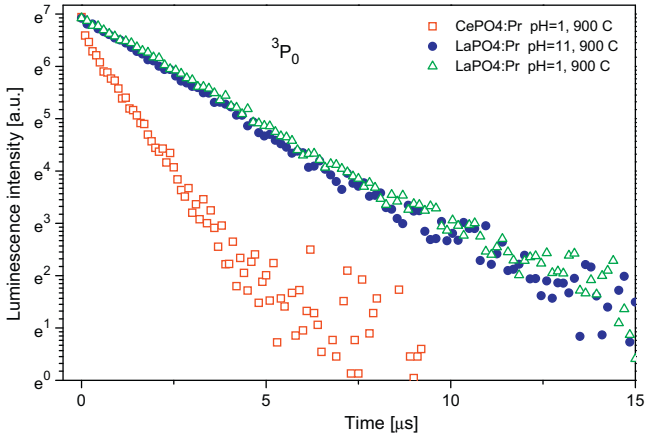

Fig. 11. Lifetimes of the $^3P_0$ multiplet of Pr^{3+} in lanthanum and cerium orthophosphates.

efficiency of the $^1D_2$ was not changed. It should be mentioned that Łempicki and McCollum worked with fluoride material synthesized in reduction atmosphere. The materials investigated in this work contain oxygen that might cause partial oxidation of Ce^{3+} to Ce^{4+} and reduction of efficiency of the $^1D_2$ level in $CePO_4$:Pr^{3+}.

4. Conclusions

The nanoparticles (12–30 nm) of hydrated (hexagonal) and water-free (monoclinic) phases of lanthanum and cerium orthophosphates were obtained and their optical properties were investigated. Unfortunately, the attempts to resolve the crystal structure of hexagonal phase using the routine procedure were unsuccessful – it was not possible to find the positions of water molecules. The monoclinic phase was obtained by calcination of as-synthesized hexagonal powder at temperature of 900 °C. This process is irreversible.

It is clearly shown that the morphology of nanoparticles of the cerium and lanthanum orthophosphates obtained by the hydrothermal method remained intact after changing the condition of synthesis from acidic to alkaline environment. Moreover, this morphology is stable after calcination at high temperature. It is found that pH has influence on the size of obtained particles. The change of pH from 1 to 11 resulted in the decrease of diameters of nanorods particles.

Differences between hexagonal and monoclinic nanocrystals are very well reflected in the infrared and Raman scattering spectra although influence of the environment conditions of the crystallisation is less meaningful. Similar phonon behaviour was found for both lanthanum and cerium phosphates. On the other hand, the structure differences as well as growth environment conditions of the crystallisation reactions play role in the luminescent properties.

Acknowledgements

The authors would like to thank M.Sc. E. Bukowska for X-ray measurements and M.Sc. L. Krajczyk for TEM and HRTEM studies. The Polish Ministry of Science and Higher Education supported this work under grant No. 1 P03B 078 29.

References

[1] N. Hashimoto, Y. Takada, K. Sato, S. Ibuki, J. Lumin. 48–49 (1991) 893.
[2] P. Iacconi, M. Junker, B. Guilhot, D. Huguenin, Opt. Mater. 17 (2001) 409.
[3] A. Jouini, J.C. Gacon, M. Ferid, M. Trabelsi-Ayadi, Opt. Mater. 24 (2003) 175.
[4] J.C. Gacon, K. Horchani, A. Jouini, C. Dujardin, I. Kamenskikh, Opt. Mater. 28 (2006) 14.
[5] A.J. Wojtowicz, W. Drozdowski, D. Wisniewski, J.-L. Lefaucheur, Z. Galazka, Z. Gou, T. Lukasiewicz, J. Kisielewski, Opt. Mater. 28 (2006) 85.
[6] S. Oshion, K. Kitamura, T. Shigeta, S. Horii, T. Matsuoka, S. Tanaka, H. Kobayashi, J. Electrochem. Soc. 146 (1999) 392.
[7] Y.C. Kang, E.J. Kim, D.Y. Lee, H.D. Park, J. Alloys Compd. 347 (2002) 266.
[8] I.W. Lenggoro, B. Xia, H. Mizushima, K. Okuyama, N. Kijima, Mater. Lett. 50 (2001) 92.
[9] R.P. Rao, D.J. Devine, J. Lumin. 87–89 (2000) 1260.
[10] U. Kolitsch, D. Holtstam, Eur. J. Mineral. 16 (2004) 117.
[11] R.C.L. Mooney, Acta Crystallogr. 3 (1950) 337.
[12] S. Jaulmes, Bull. Soc. Fr. Mineral. Crystallogr. 95 (1972) 42.
[13] G.W. Beall, L.A. Boatner, D.F. Mullica, W.O. Miligan, J. Inorg. Nucl. Chem. 43 (1981) 101.
[14] Y. Ni, J.M. Hughes, A.N. Mariano, Am. Mineral. 80 (1995) 21.
[15] Y.P. Fang, A.W. Xu, R.Q. Song, H.X. Zhang, L.P. You, J.C. Yu, H.Q. Liu, J. Am. Chem. Soc. 125 (2003) 16025.
[16] M. Yang, H. You, G. Jia, Y. Huang, Y. Song, Y. Zheng, K. Liu, L. Zhang, J. Cryst. Growth 311 (2009) 4753.
[17] S. Lucas, E. Champion, D. Bernache-Assollant, G. Leroy, J. Solid State Chem. 177 (2004) 1312.
[18] I. Khorvath, I.A. Bondar, L.P. Mezentseva, Zh. Neorg. Khim. 31 (1986) 2250; I. Khorvath, I.A. Bondar, L.P. Mezentseva, J. Thermal Anal. 33 (1988) 755.
[19] J.A. Diaz-Guillen, A.F. Fuentes, S. Gallini, M.T. Colomer, J. Alloys Compd. 427 (2007) 87.
[20] M. Ferhi, K. Hotchani-Naifer, M. Ferid, J. Lumin. 128 (2008) 1777.
[21] Y.P. Fang, A.W. Xu, W.F. Dong, Small 1 (2005) 967.
[22] Y. Zhang, H. Guan, J. Cryst. Growth 256 (2003) 156.
[23] Y. Zhang, H. Guan, Mater. Res. Bull. 40 (2005) 1536.
[24] A. Boultif, D. Louer, J. Appl. Crystallogr. 37 (2004) 724, DICVOL04 – Powder diffraction pattern indexing, ver. July 2004.
[25] J. Rodriguez-Carvajal, Commission on Powder Diffraction (IUCr) Newsletter 26 (2001) 12–19, http://journals.iucr.org/iucr-top/comm/cpd/Newsletters/.
[26] A.L. Patterson, Phys. Rev. 56 (1939) 978.
[27] S. Chattopadhyay, P. Ayyub, V.R. Palkar, M. Multani, Phys. Rev. B 52 (1995) 13177.
[28] F. Toney, J. Gijo, M. Siby, P.R. Rejikumar, N.V. Unnikrishnan, J. Sol–Gel Sci. Technol. 41 (2007) 163.
[29] M. Inokuti, F. Hirayama, J. Chem. Phys. 43 (1965) 1978.
[30] S. Tie, Q. Su, Y. Yu, J. Alloys Compd. 227 (1995) 1.
[31] R.C.L. Mooney, J. Chem. Phys. 16 (1948) 1003.
[32] J.A. Salthose, M.J. Ware, Point Group Character Tables, Cambridge, 1972.
[33] J. Lin, G. Yao, Y. Dong, B. Park, M. Su, J. Alloys Compd. 225 (1995) 124.
[34] A. Paulenova, S.E. Creager, J.D. Navratil, Y. Wei, J. Power Sources 109 (2002) 431.
[35] A. Łempicki, B.C. McCollum, J. Lumin. 20 (1979) 291.